





## Original Article

# Interventional Effects of Grape Skin Extract against Lung Injury Induced by Artificial Fine Particulate Matter in a Rat Model



Zhigang Liu<sup>1,2#</sup>, Sizheng Li<sup>2#</sup>, Yahao Ling<sup>3</sup>, Haiyan Jiang<sup>2</sup>, Lian Kuang<sup>2</sup>, Jie Bao<sup>2,4</sup>, Jing Li<sup>1,5</sup>, Peicheng Zhang<sup>6\*</sup>  and Hongtao Jin<sup>2,4,7\*</sup> 

<sup>1</sup>School of Biology and Biological Engineering, South China University of Technology, Guangzhou, China; <sup>2</sup>New Drug Safety Evaluation Center, Institute of Materia Medica, Chinese Academy of Medical Sciences and Peking Union Medical College, Beijing, China; <sup>3</sup>Department of Pharmacy, People's Hospital of Longhua District Shenzhen, Guangdong, China; <sup>4</sup>Beijing Union-Genius Pharmaceutical Technology Development Co. Ltd., Beijing, China; <sup>5</sup>Department of Pulmonary and Critical Care Medicine, Guangdong Provincial People's Hospital, Guangdong Academy of Medical Sciences, Guangzhou, Guangdong, China; <sup>6</sup>Chinese Academy of Medical Sciences and Peking Union Medical College, Institute of Materia Medica, State Key Laboratory of Bioactive Substance and Function of Natural Medicines, Beijing, China; <sup>7</sup>NMPA Key Laboratory for Safety Research and Evaluation of Innovative Drug, Beijing, China

Received: July 01, 2022 | Revised: July 19, 2022 | Accepted: August 24, 2022 | Published: October 26, 2022

## Abstract

**Background and objectives:** The mechanism underlying lung injury due to atmospheric fine particulate matter (PM<sub>2.5</sub>) remains unclear, and currently, there are no medications for specific intervention.

**Methods:** Different doses of grape skin extract (GSE, 0.1, 0.2, and 0.4 g/kg, respectively) were administered prophylactically to the treatment groups, while sterile water was administered to the control and model groups. PM<sub>2.5</sub> in suspension (1 mL at 30 mg/kg) was administered twice weekly for six weeks. The rats were sacrificed 48 h after the last administration. Pulmonary function was assessed weekly by a whole-body plethysmography system. Hematoxylin-eosin staining, alveolar lavage fluid leukocyte classification and counts, detection of cytokines with an enzyme-linked immunosorbent assay, and other methods were employed to evaluate pathological changes and inflammation of the lungs, amino acid metabolomics, and lipid metabolomics. A gene chip was used for mRNA profiling to identify potential drug targets.

**Results:** Lung function was diminished compared to the control group. Pathological changes were significant, and lung inflammation was more evident in the model group. There were also apparent changes in lung tissues and serum metabolites

of amino acids and lipids. The lung function, the inflammatory response, fibrosis, and the number of phagocytes of the lung interstitium were significantly improved with GSE treatment. Local inflammation of lung tissue was reduced. Serum, lung tissue amino acids, and lipid metabolites underwent dramatic corrections. Functional enrichment analysis found that GSE improved the lung damage caused by PM<sub>2.5</sub> via the complement and oxidative phosphorylation pathways.

**Conclusions:** GSE significantly improved lung injury and pulmonary inflammation induced by PM<sub>2.5</sub> in rats. The detection results of multiple omics provided important information for subsequent comprehensive clarification of potential targets and intervention mechanisms of GSE.

**Keywords:** Grape skin extract; Artificial fine particulate matter; Lung injury; Interventional effect.

**Abbreviations:** BALF, bronchoalveolar lavage fluid; DEGs, differentially expressed genes; EIP, End-inspiratory pause; EF50, 50% tidal volume; GSE, grape skin extract; MV, minute ventilation volume; PEF, peak expiratory flow; PM, particulate matter; RT, relaxation time; Te, expiratory time; Ti, inspiratory time; TNF- $\alpha$ , tumor necrosis factor alpha.

\***Correspondence to:** Peicheng Zhang, Chinese Academy of Medical Sciences and Peking Union Medical College, Institute of Materia Medica, State Key Laboratory of Bioactive Substance and Function of Natural Medicines, Beijing 100050, China. ORCID: <https://orcid.org/0000-0002-0739-0019>. Tel: 010-63165231, Fax: 010-63017757, E-mail: [pczhang@imm.ac.cn](mailto:pczhang@imm.ac.cn); Hongtao Jin, New Drug Safety Evaluation Center, Institute of Materia Medica, Chinese Academy of Medical Sciences and Peking Union Medical College, Beijing 100050, China. ORCID: <https://orcid.org/0000-0002-0638-707X>. Tel: 010-67817730, Fax: 010-67817731, E-mail: [jinhongtao@imm.ac.cn](mailto:jinhongtao@imm.ac.cn)

#These authors equally contributed to this work.

**How to cite this article:** Liu Z, Li S, Ling Y, Jiang H, Kuang L, Bao J, *et al.* Interventional Effects of Grape Skin Extract against Lung Injury Induced by Artificial Fine Particulate Matter in a Rat Model. *Future Integr Med* 2022;1(1):2–12. doi: 10.14218/FIM.2022.00030.

## Introduction

Environmental pollution has always been catastrophic for human health, causing severe medical hazards in different countries and regions. PM<sub>2.5</sub> enters the body from the respiratory tract, deposits in the bronchi and alveoli, and involves the respiratory,<sup>1</sup> cardiovascular,<sup>2</sup> digestive systems,<sup>3</sup> *etc.* PM<sub>2.5</sub> had significant adverse effects on the incidence of lung cancer in both men and women in China.<sup>4</sup> It can also cause respiratory diseases, such as airway hyperreactivity, chronic obstructive pulmonary disease, and allergic asthma. The study found that 253 premature deaths per million population were associated with exposure to environmental PM<sub>2.5</sub>.<sup>5</sup> Ambient PM<sub>2.5</sub>-attributable non-communicable diseases have threatened public health in middle and low socio-demographic index countries, while household PM<sub>2.5</sub>-attributable lower respiratory infections still cause an enormous burden in low socio-demographic index countries.<sup>6</sup> PM<sub>2.5</sub> entering the lungs will also activate alveolar macrophages, leading to overproduction of reactive oxygen species and the release of pro-inflammatory cytokines, which activate a series of complex immune responses that reduce lung function and cause histopathological changes, resulting in aggravation of asthma and chronic obstructive pulmonary disease (COPD). Airway epithelial cells are responsible for maintaining homeostasis in the lungs, along with alveolar macrophages, which play an essential role in the clearance of foreign bodies.<sup>7</sup> Therefore, it would be helpful to elucidate the mechanisms underlying PM<sub>2.5</sub>-induced damage to the respiratory tract to take adequate measures, including drug protection, especially for traditional Chinese medicine.

The main components of grape skin extract (GSE) include gallic acid, protocatechuic acid, catechuic acid, epicatechin, and resveratrol. Our group previously reported that resveratrol glycoside (polydatin) significantly alleviated lung function reduced by atmospheric exposure to fine PM<sub>2.5</sub> and lung inflammation in rats, demonstrating strong antioxidant and anti-inflammatory activities.<sup>8</sup> In addition, polyphenols of grape skin have been shown to scavenge free radicals and antioxidants. Therefore, the present study aimed to investigate the effects of GSE against PM<sub>2.5</sub>-induced lung damage and to explore the underlying protective mechanisms in the lung injury rat model.

## Materials and methods

### Primary reagents and instruments

The primary reagents and instruments used in this study included GSE (production number: 20160812, Institute of Materia Medica, Chinese Academy of Medical Sciences), PM<sub>2.5</sub> (Institute of Materia Medica, Chinese Academy of Medical Sciences), AccQ derivative (Waters Corporation, Milford, MA, USA), AccQ borate buffer (Waters Corporation), hematoxylin dyeing solution (Shanghai Beyotime Biotechnology Co., Ltd., Shanghai, China), Eosin staining solution (Shanghai Beyotime Biotechnology Co., Ltd.), a whole body plethysmography system (EMKA TECHNOLOGIES, Paris, France), automatic hemocytometer (MEK-7222K, Nihon Kohden Corporation, Tokyo, Japan), bioanalyzer (Model 2100, Agilent Technologies, Inc., Santa Clara, CA, USA), spectrophotometer (NanoDrop 1000, Thermo Fisher Scientific, Waltham, MA, USA), PCR System (7900 HT, Applied Biosystems, Carlsbad, CA, USA), and microarray scanner (Agilent).

### Laboratory animals and interventions

Sprague Dawley rats were purchased from Beijing Vital River Laboratory Animal Technology Co., Ltd. (Beijing, China) and

housed in a specific-pathogen-free animal care facility under a constant temperature of 20–26 °C, relative humidity of 40–70%, and 12 h light/dark cycle with *ad libitum* access to standard chow and water. The animal test has been approved by the Center for Beijing Union-Genius Pharmaceutical Technology Development Co. Ltd. Ethical Approval No.: 2017-0000242. Following a brief acclimation period, the rats were randomly divided into five groups, including the control group, model group, low-dose GSE group (0.1 g/kg), medium-dose GSE group (0.2 g/kg), and high-dose GSE group (0.4 g/kg), with eight rats in each group. Rats in the control and model groups were administered intragastrically with sterile water. After four days of intragastric administration, the trachea of all rats was instilled with PM<sub>2.5</sub> at 30 mg/kg body weight twice per week for six weeks.

## Research methodology

### Lung function measurement by whole-body plethysmography

Rats were measured awake by a whole-body plethysmography system to assess lung function.<sup>9</sup> After adjusting relevant parameters for instrument calibration, the rats were placed in a “tracing box” for 5–10 min until stabilized. Then, the lung function of all rats was measured with the whole-body volume tracing system once per week. Significant changes in lung function were identified between the model and control groups, concluding the investigation.

### Hematoxylin-eosin staining

All rats' left lungs were collected under anesthesia (2% sodium pentobarbital, 40 mg/kg), then soaked in 4% paraformaldehyde for 48 h, dehydrated, paraffin-embedded, sliced, dewaxed, hydrated, stained with hematoxylin and eosin, dehydrated again, cleared with xylene, dried, sealed with neutral gum, and photographed under a microscope.

### Measurement of cell fractions in bronchoalveolar lavage fluid (BALF)

After the pulmonary function test, the rats were treated with thoracotomy, and the left bronchus was isolated and ligated. BALF was collected by lavage three times with 2 mL precooled phosphate buffer saline. BALF was collected to measure the percentages of white blood cells, lymphocytes, neutrophils, basophils, eosinophils, and monocytes.

### Measurement of inflammatory factors in BALF

Interleukin (IL)-1 and IL-10 levels were measured using the Bio-Plex Pro™ Rat Cytokine Detection Kit (Bio-Rad Laboratories, Hercules, CA, USA) in accordance with the manufacturer's instructions. Briefly, 50-μL aliquots of the samples were combined with 50 μL of anti-cytokine antibody detection beads per well, washed twice, and mixed with buffer. Corresponding wells were used to construct a standard curve. Following incubation for 30 min at room temperature on a shaker at 500 rpm in the dark and, after washing three times, the detection antibody (25 μL) and streptavidin-phycoerythrin fluorescent pigment (50 μL) were added sequentially. The beads were resuspended in 125 μL of buffer per well, placed into the Bio-Plex 200 liquid phase protein chip analysis system, and the fluorescence intensity of each well was measured to calculate the concentrations of IL-1β and IL-10 in the sample against the fluorescence intensity of the standard.

### Metabolomics analysis of amino acids in lung tissue and serum

The samples were fractionated using a Waters XBridge Peptide BEH

**Table 1. Mass spectrum parameters**

Parameters	TOF MS(+)	Product Ion(+)	IDA
Ion Source Gas 1	50	50	
Ion Source Gas 2	50	50	
Curtain Gas	30	30	
Temperature	550	550	
IonSpray Voltage Floating	5,500	5,500	
TOF Masses	200–700	50–700	
Declustering Potential	80	80	
Collision Energy	10	30	
Collision Energy Spread	–	15	
Ion Release Delay	–	63	
Ion Release Width	–	23	

IDA, information-dependent acquisition; MS, mass spectrometry; TOF, time of flight.

C18 column (3.5  $\mu\text{m}$ , 2.1 $\times$ 100 mm). The mobile phase for amino acid detection in lung tissue consisted of (A) 10 mM ammonium formate + 0.1% formic acid + 99.9% water, and (B) 1.6% formic acid + 98.4% acetonitrile. The mobile phase for serum amino acid detection consisted of (A) 20 mM ammonium formate+0.5% formic acid + 1% acetonitrile + 98.5% water, and (B) 1.6% formic acid + 98.4% acetonitrile. The mass spectrometry parameters are shown in Table 1.

#### Lipid metabolomics analysis of lung tissue

Lung tissue samples (about 20 mg) were homogenized in 200  $\mu\text{L}$  of  $\text{H}_2\text{O}$  for 3 min, then mixed with a volumetric solution mixture (10  $\mu\text{L}$ , 3  $\mu\text{g}/\text{mL}$ ) and vortexed for 10 s. After adding 800  $\mu\text{L}$  of protein extract (chloroform: methanol=2:1), the samples were vortexed for 2 min and then allowed to stand for 30 min. After centrifugation (13,000 g, 5 min), the chloroform layer was removed using a syringe (1 mL) and divided into two aliquots of 100  $\mu\text{L}$ , which were dried under a stream of  $\text{N}_2$  gas and then re-dissolved. Finally, 25  $\mu\text{L}$  aliquots of each sample were analyzed by chromatography under the following conditions: column temperature, 50  $^\circ\text{C}$ ; injection chamber temperature, 4  $^\circ\text{C}$ ; flow rate, 0.4 mL/min; and injection volume, 2  $\mu\text{L}$ . The mobile phase consisted of (A) 10 mM ammonium acetate + 0.1% carboxylic acid + 99.9% water, and (B) 10 mM ammonium acetate + 0.1% formic acid + 49.95% acetonitrile + 49.95% isopropanol. The gradient elution conditions are shown in Table 2, and the mass spectrometry conditions are shown in Tables 3 and 4.

#### Gene chip monitoring of mRNA expression profiles

Profiles of mRNA expression were examined by gene chip tech-

**Table 2. Gradient elution condition**

Time(min)	A%	B%
0.01	95	5
15	60	40
17	0	100
20	0	100
20.5	95	5
25	95	5

**Table 3. Positive and negative ion mode**

Parameters	TOF MS(+)/(-)	Product Ion(+)/(-)	IDA
Ion Source Gas 1	50	50	
Ion Source Gas 2	50	50	
Curtain Gas	30	30	
Temperature	550	550	
Ion Spray Voltage Floating	5,500/4,500	5,500/4,500	
TOF Masses	100–1,500/100–1,200	50–1,200	
Declustering Potential	80/–80	80/–80	
Collision Energy	10/–10	35/–35	
Collision Energy Spread	–	15	
Ion Release Delay	–	67	
Ion Release Width	–	25	

IDA, information-dependent acquisition; MS, mass spectrometry; TOF, time of flight.

nology. Total RNA was extracted using TRIzol reagent (Invitrogen Corporation, Carlsbad, CA, USA), and the quality was evaluated with a microplate reader at wavelengths of 260, 280, and 230 nm. Qualified total RNA was separated by agarose gel electrophoresis. The RNA samples' concentration, purity, and integrity were determined with a bioanalyzer (Agilent Technologies, Inc.). The RNA integrity number, as a quality index, was calculated following the instructions of the Agilent RNA 6000 Nano Kit. The resulting quality mRNA was prepared for further analysis (cDNA synthesis, antisense RNA synthesis, fluorescent labeling, and hybridization).

#### Data acquisition

The amino acid metabolomics results were based on an amino acid standard database. Peak area data were obtained with PeakView1.2 software (AB SCIEX, Concord, ON, Canada) to characterize amino acids in lung tissue and serum samples, which were then quantified with MultiQuant2.1 software (AB SCIEX) (Table 5).

Lipid metabolomics was conducted to characterize lipids in lung tissue samples in reference to the Lipid Standard Database using PeakView 1.2 software and then quantified based on peak area data with MultiQuant2.1 software (Table 6).

The mRNA profile data obtained from the gene chip results were processed using the Rosetta Resolver<sup>®</sup> gene expression data analysis system (Rosetta Biosoftware, Seattle, WA, USA), which included data screening and correction and statistical calculations. The differential gene expression analysis results are log<sub>2</sub> (ratio)

**Table 4. Gradient elution conditions**

Time (min)	A%	B%
0.01	65	35
2	20	80
9	0	100
15	0	100
16	65	35
20	65	35

**Table 5. The amino acid metabolomics MultiQuant 2.1 parameters.**

Parameter	Positive ions
Mass-to-charge ratio (m/z)	±0.0025
Gaussian smooth width	2 points
RT half window	10 sec
Min. peak width	3 points
Min. peak height	100
Noise percentage	5%
Baseline sub. Window	2.00 min
Peak splitting	2 points

RT, retention time.

values, with a positive value indicating upregulation and a negative value indicating downregulation. The log<sub>2</sub> (ratio) and multiple (fold change) conversion relationship was calculated as follows: Fold change=2 log<sub>2</sub> (ratio). Probes with significantly different performances were selected according to log<sub>2</sub> (ratio) and *p*-value (differentially expressed). Log<sub>2</sub> (ratio) ≥1 and *p*-value (differentially expressed) <0.05 were the predetermined conditions for identifying differential expression. Principal component analysis was conducted with the built-in “prcomp” function, and cluster analysis was performed with the “amap,” “ctc,” “gplots,” and other packages included with the Rosetta Biosoftware suite. If the difference in gene expression was too small for analysis with Rosetta Biosoftware, analysis of variance was performed to identify differentially expressed genes (DEGs) (*p*<0.05).

### Statistical analysis

The data were processed with Excel 2013 software (Microsoft Corporation, Redmond, WA, USA). The results are expressed as the mean±standard deviation or standard error. Homogeneity among the groups was assessed using the F-test, and significance between two groups was identified with the two-sided Student's *t*-test. A probability (*p*) value of <0.05 was considered statistically significant. Images were created with GraphPad Prism 5.0 software (GraphPad Software, Inc., San Diego, CA, USA).

## Results

### GSE could significantly improve PM2.5-induced lung injury

End-inspiratory pause (EIP), inspiratory time (Ti), and expiratory time (Te) were considerably lowered in the model group compared to the control group, whereas respiratory rate (f) and minute ventilation volume (MV) rose significantly (*p*<0.01). In addition, relaxation time (RT) was reduced dramatically, while peak expiratory flow (PEF) and expiratory air velocity at 50% tidal volume (EF50) were significantly increased. Overall, the pulmonary function indicators f, MV, EF50, PEF, and PIF had increased, and RT, Te, Ti, and EIP had decreased, confirming that the model was successfully established. Treatment with GSE significantly improved lung function, as indicated by significant reductions in the pulmonary function indicators f, MV, EF50, PEF, and PIF, and significant increases in RT, Te, Ti, and EIP. Changes to lung function indicators in each group are illustrated in Figure 1.

The histopathological results in Figure 2 showed that the lung tissue structure was relatively complete in the control group, with

**Table 6. Lipid metabolomics MultiQuant 2.1 parameters**

Parameter	Positive ions	Negative ion
Mass-to-charge ratio (m/z)	±0.0025	±0.0025
Gaussian smooth width	2 points	2 points
RT half window	10 sec	10 sec
Min. peak width	3 points	3 points
Min. peak height	100	100
Noise percentage	5%	5%
Baseline sub. Window	2.00 min	2.00 min
Peak splitting	2 points	2 points

RT, retention time.

a comparatively uniform distribution of alveoli and no significant morphological change. In the model group, the alveolar space was widened, infiltration of granulocytes and lymphocytes was significantly increased, the alveoli were highly expanded, the alveolar walls were severely ruptured and fused, and some alveoli consolidation was observed. In the high-dose GSE group, the spacing of alveoli was relatively increased, inflammation was significantly reduced, the alveolar structure tended to be intact, the alveoli were dilated, the number of phagocytes was reduced, and the extent of lesions was significantly improved as compared to the model group. However, there was no significant improvement in lung tissue damage in the low- and medium-dose GSE groups compared to the model group.

### GSE could significantly improve PM2.5-induced inflammation

Compared to the control group, the percentages of white blood cells, lymphocytes, neutrophils, and eosinophils were significantly increased in BALF of the model group (*p*<0.01). The percentage of neutrophils in the medium- and high-dose GSE groups was substantially lower than in the control group (*p*<0.05). Further analysis showed that after six weeks of PM2.5 instillation, the percentage of lymphocytes had significantly increased in the model group (*p*<0.05), and the percentage of basophils had significantly decreased (*p*<0.05) as compared to the control group. Overall, GSE treatment tended to augment the proportion of basophils. The percentage of leukocytes in BALF of each group is shown in Figure 3.

An ELISA (Bio-Plex Pro™ Rat Cytokine Detection Kit) was used to detect the expression levels of IL-1β and IL-10 in BALF. The results showed that the IL-1β content was considerably higher in the model group than in the control group (*p*<0.01) and significantly reduced in each GSE-treatment group as compared to the model group (*p*<0.05) (Fig. 4a). In addition, the content of IL-10 in rat BALF was significantly reduced in the model group as compared to the control group (*p*<0.05), while there was no significant difference between the GSE-treatment groups and the model group (Fig. 4b).

### GSE reduced PM2.5-induced dysregulation of amino acid metabolism

Compared to the control group, the contents of 4-hydroxy-*l*-proline and *l*-arginine were significantly reduced in the lung tissue of rats in the model group (Fig. 5). Compared to the model group, there were no significant differences in the contents of 4-hydroxy-*l*-proline and *l*-arginine in rat lung tissue among the GSE-treatment

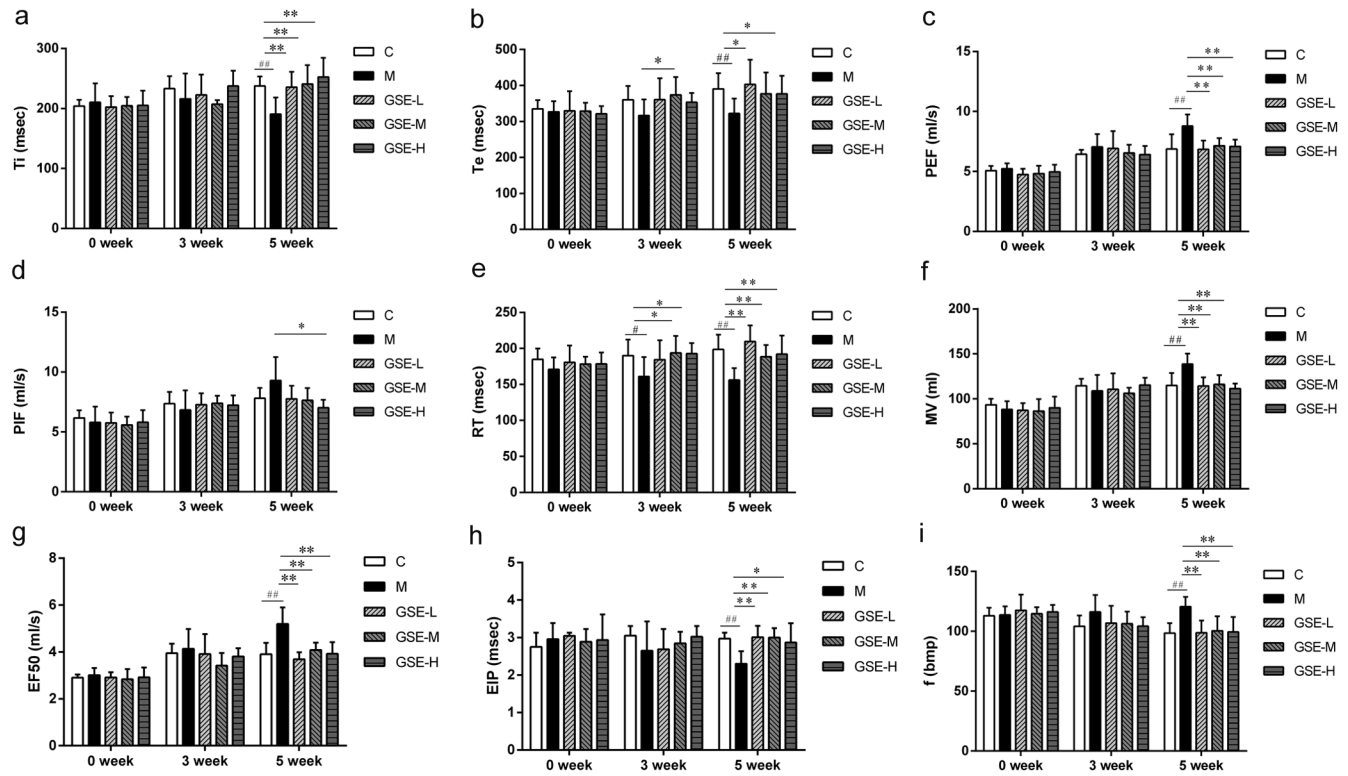


**Fig. 1. Dynamic monitoring of lung function.** C, control group; M, model group; GSE-L, low-dose GSE group; GSE-M, medium-dose GSE group; GSE-H, high-dose GSE group. # $p < 0.05$ , ### $p < 0.01$  vs. the control group; \* $p < 0.05$ , \*\* $p < 0.01$  vs. the model group. (a) Inspiratory time,  $T_i$ . (b) expiratory time,  $T_e$ . (c) Peak expiratory flow, PEF. (d) Peak inspiratory flow, PIF. (e) Relaxation time, RT. (f) Minute ventilation, MV. (g) Maximal expiratory flow rate at 50% vital capacity, EF50. (h) End-inspiratory pause, EIP. (i) Respiratory rate, f. EF50, the maximal expiratory flow rate at 50% vital capacity; EIP, end-inspiratory pause; f, respiratory rate; MV, minute ventilation; PEF, peak expiratory flow; PIF, peak inspiratory flow; RT, relaxation time;  $T_e$ , expiratory time;  $T_i$ , inspiratory time.

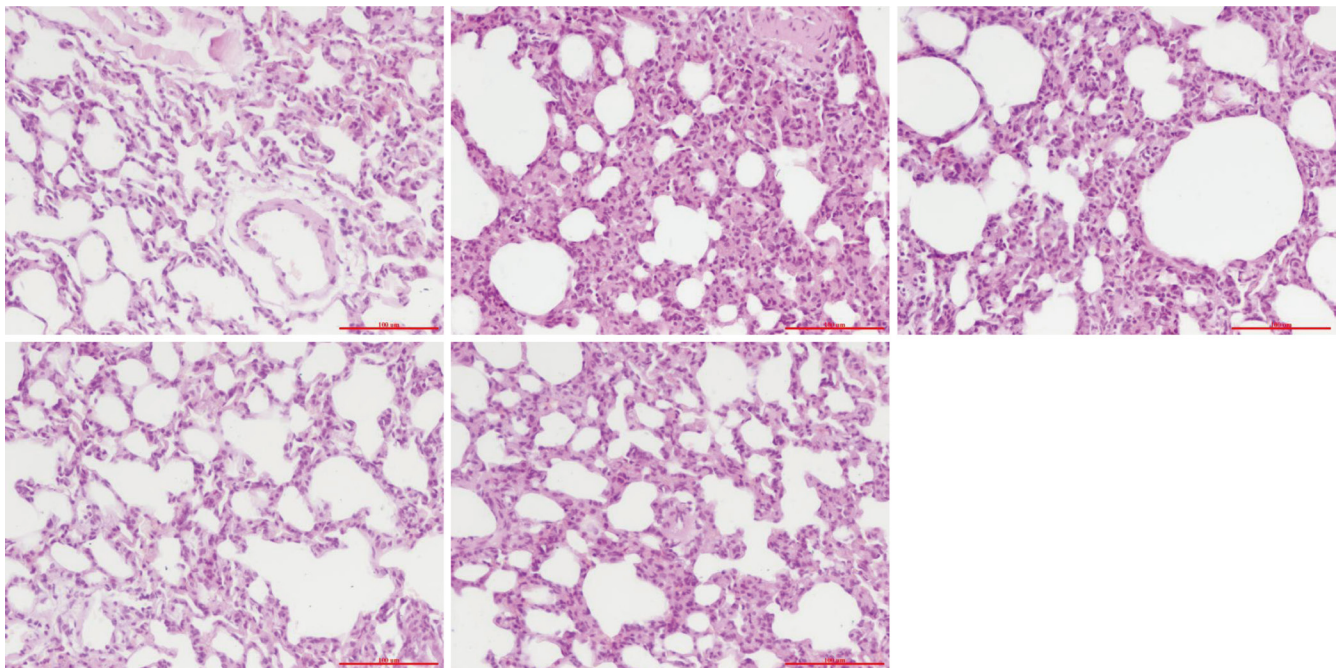


**Fig. 2. Lung histopathology.** (a) Control group; (b) Model group; (c) Low-dose GSE group; (d) Medium-dose GSE group; (e) High-dose GSE group (magnification,  $\times 200$ ). GSE, grape skin extract.

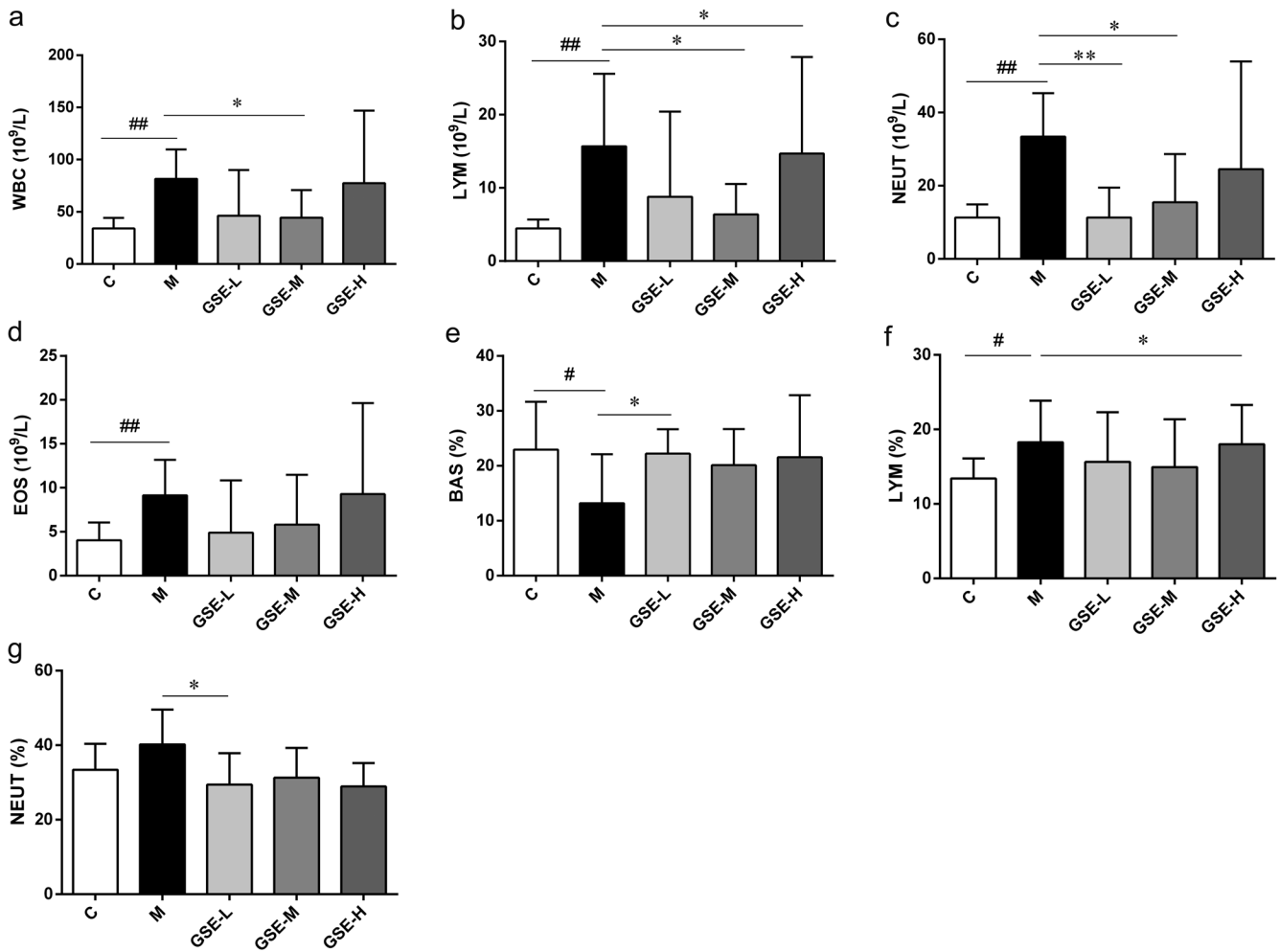


**Fig. 3. Cell fractions in BALF.** C, control group; M, model group; GSE-L, low-dose GSE group; GSE-M, medium-dose GSE group; GSE-H, high-dose GSE group. #*p*<0.05, ##*p*<0.01 vs. the control group; \**p*<0.05, \*\**p*<0.01 vs. the model group. (a) White blood cells, WBC; (b) Lymphocytes, LYM; (c) Neutrophils, NEUT; (d) Eosinophils, EOS; (e) Basophil percentage, BAS%; (f) Lymphocyte percentage, LYM%; (g) Neutrophil percentage, NEUT%. BALF, bronchoalveolar lavage fluid; BAS%, basophil percentage; EOS, eosinophils; GSE, grape skin extract; LYM, lymphocytes; LYM%, lymphocyte percentage; NEUT, neutrophils; NEUT%, neutrophil percentage; WBC, white blood cells.

groups, although levels tended to increase with GSE dosage. As compared to the control group, serum levels of pipecolic acid, *l*-phenylalanine, and hypotaurine were significantly increased in the

model group (*p*<0.05). Compared to the model group, serum levels of *l*-phenylalanine and hypotaurine were significantly reduced in the high and low-dose GSE group (*p*<0.01 and *p*<0.05, respectively).

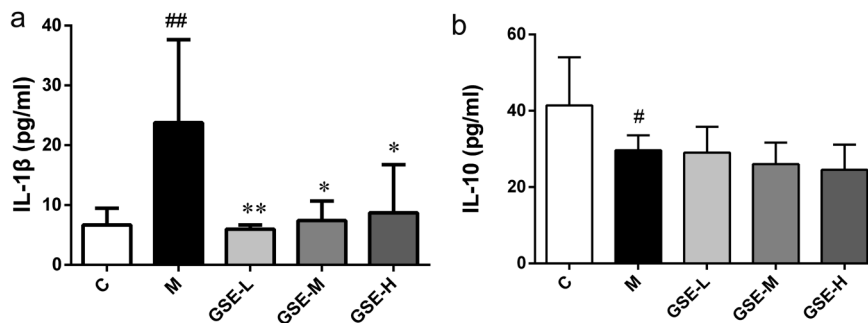


**Fig. 4. Responses of inflammatory factors to GSE.** C, control group; M, model group; GSE-L, low-dose GSE group; GSE-M, medium-dose GSE group; GSE-H, high-dose GSE group. #*p*<0.05, ##*p*<0.01 vs. the control group; \**p*<0.05, \*\**p*<0.01 vs. the model group. (a) Interleukin-1β, IL-1β; (b) Interleukin-10, IL-10. GSE, grape skin extract; IL-1β, Interleukin-1β; IL-10, Interleukin-10.

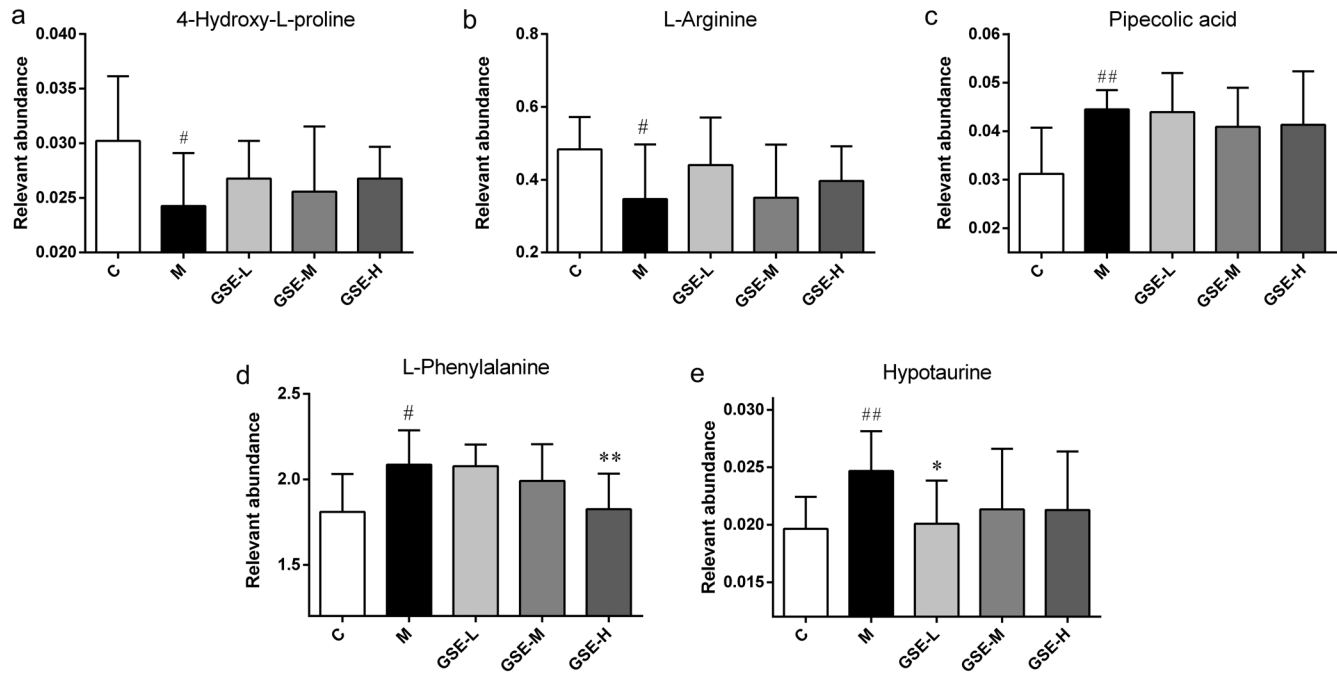


**Fig. 5. Relative abundance of amino acids in lung tissue and serum of rats after PM2.5 instillation.** C, control group; M, model group; GSE-L, low-dose GSE group; GSE-M, medium-dose GSE group; GSE-H, high-dose GSE group. #*p*<0.05, ##*p*<0.01 vs. the control group; \**p*<0.05, \*\**p*<0.01 vs. the model group. (a) 4-hydroxy-*l*-proline in lung tissue. (b) *l*-arginine in lung tissue. (c) Pipecolic acid in serum. (d) *l*-phenylalanine in serum. (e) Hypotaurine in serum. GSE, grape skin extract.

**GSE altered lipid metabolism in rats with lung injury**

The concentration of 1,2-palmitoyl-SN-glycerol-3-phosphocholine in the lung tissue of rats in the model group was substantially lower than in the control group (*p*<0.01). In contrast, the content of 1-tetradecane-2-hydroxy-SN-glycerol-3-phosphoglyphobylline was significantly elevated (*p*<0.05). Meanwhile, the contents of 1,2-palmitoyl-SN-glycerol-3-phosphocholine and 1-stearoyl-2-hydroxy-SN-glycerol-phosphate inositol were significantly elevated in the lung tissues of rats in the GSE-treatment groups (*p*<0.05), while the contents of hemolytic phosphatidylcholine, including 1-arachidyl-2-hydroxy-SN-glycerin-3-phosphocholine, 1-behen-2-hydroxy-SN-glycerin-3-phosphocholine, and 1-tetradecane-2-hydroxy-SN-glycerin-3-phosphocholine, tended to decrease (*p*<0.05). The lipid contents in lung tissues of rats in each group are shown in Figure 6.

**Identification of DEGs by mRNA expression profiling**

The histogram (left) shows the distribution of signal differences in all detected gene probes (excluding control and flagged probes) among the groups. The abscissa of the histogram is the log2 value of the degree of difference, and the ordinate represents the number of probes. The volcano plot (right) shows the distribution of differential gene probes among the groups. The degree of difference (log2) is shown along the abscissa, and the negative log (*p*-value), representing the significance of the difference, is shown along the ordinate. The red/green dotted lines represent the *p*-value and multiple filtering thresholds, respectively. Each point in the figure is a detected gene probe (excluding control and flagged probes). The parameters for identifying DEGs were log2 (ratio) ≥1 and *p*<0.05. Representative results are presented in the form of histograms and volcano plots presented in Figure 7.

**Results of functional enrichment analysis**

Enrichment analysis showed that the signaling pathways associated with the DEGs in the model and control groups included the chemokine signaling pathway, tumor necrosis factor signaling pathway, peroxisome proliferation activated receptor signaling pathway, lipolysis regulatory signaling pathway of fat cells, and adenosine monophosphate-dependent protein kinase signaling pathway. In addition, the signaling pathways associated with the DEGs between the GSE-treatment and model groups included oxidative phosphorylation and complement system pathways.

**Discussion**

The respiratory system’s primary function is exchanging gases with the external atmosphere. Inhalation of particles suspended in the atmosphere can lead to lung damage and aggravation of respiratory diseases. Upon entering the respiratory tract, PM2.5 stimulates hyperemia, edema, and mucus secretion by the mucosa, while increasing bronchial hyperreactivity and weakening physiological function, manifesting as decreased lung function. Lung function is a crucial indicator of the state of the respiratory system. Studies have shown that PM2.5 exposure is positively associated with decreased lung function.<sup>10-12</sup>

In this study, the toxicity of PM2.5 in suspension was assessed using a rat model. Biopsy of exposed rats showed broad alveolar septa, pulmonary interstitial cell hyperplasia to different extents, increased alveolar height, severe fracturing of the alveolar wall, and alveolar fusion, accompanied by prominent infiltration of granulocytes and lymphocytes. Notably, the deposition of PM2.5, which eventually causes inflammation and airflow obstruction, exacerbated these effects. The lung function indicators f, MV, EF50,

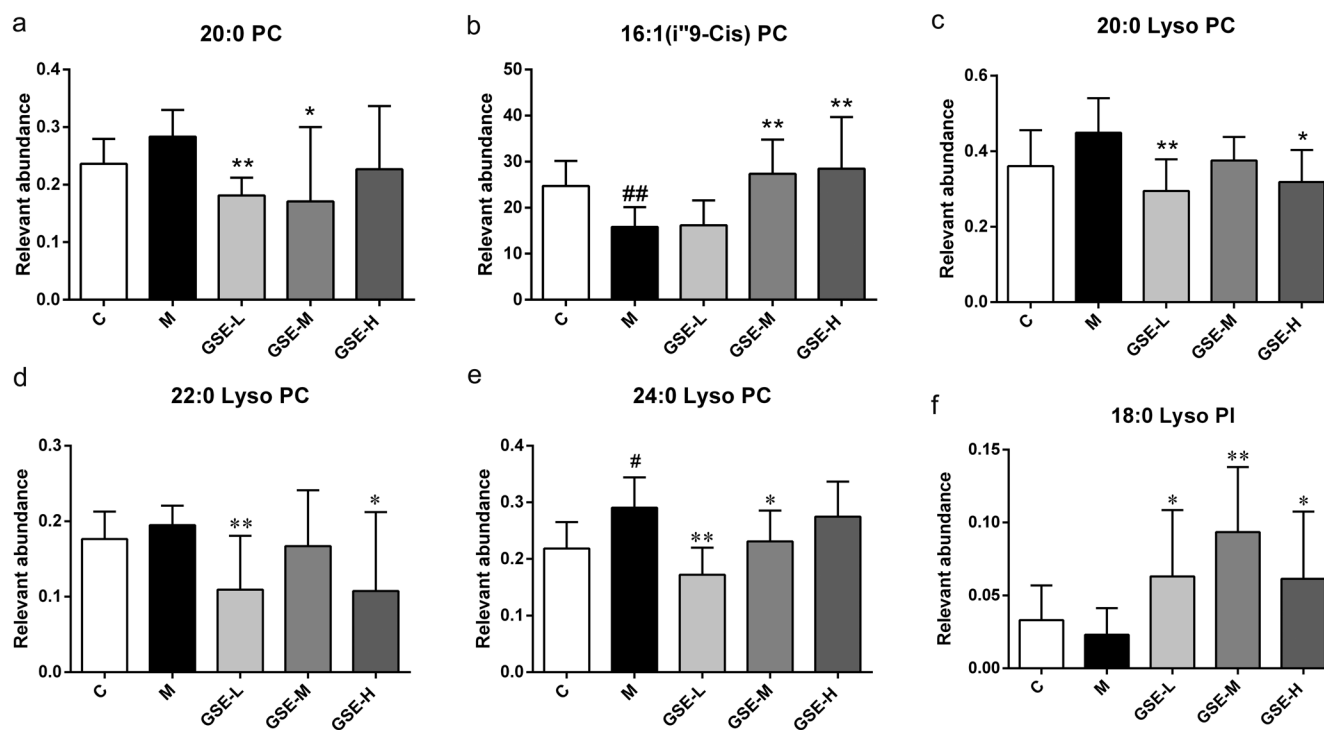


**Fig. 6. Lung tissue lipid assay results.** C, control group; M, model group; GSE-L, low-dose GSE group; GSE-M, medium-dose GSE group; GSE-H, high-dose GSE group. # $p < 0.05$ , ## $p < 0.01$  vs. the control group; \* $p < 0.05$ , \*\* $p < 0.01$  vs. the model group. (a) 1,2-Diazanoyl-SN-glycerin-3-phosphocholine (20:0 PC). (b) 1,2-Palmitoyl-SN-glycerin-3-phosphocholine (16:1(i''9-Cis)PC). (c) 1-Arachidyl-2-hydroxy-SN-glycerin-3-phosphocholine (20:0 Lyso PC). (d) 1-Behen-2-hydroxy-SN-glycerol-3-phosphocholine (22:0 Lyso PC). (e) 1-Tetradecane-2-hydroxy-SN-glycerin-3-phosphocholine (24:0 Lyso PC). (f) 1-Stearoyl-2-hydroxy-SN-glycerin-phosphate inositol (18:0 Lyso PI). GSE, grape skin extract.

and PEF of rats in the model group were significantly increased relative to the control group, while EIP, RT, Te, and Ti were reduced. Moreover, the volume and flow rate indices had increased while the time index had decreased, indicating that lung ventilation had decreased and airflow was blocked, which may be related to the pathological manifestation of high alveolar expansion and alveolar wall rupture and fusion.<sup>13,14</sup> Notably, GSE intervention significantly improved these indicators of lung function.

Bronchoalveolar lavage is the primary technical method employed to study the cellular and soluble components of the alveolar epithelial surface fluid.<sup>15</sup> The characteristics and extent of lung lesions are determined by analyzing BALF.<sup>16</sup> Eosinophils are essential effector cells of airway inflammation in asthma. However, increasing the number of cells causes tissue damage and promotes inflammation. In addition, the activity of neutrophils and lymphocytes is critical for maintaining normal lung function. However, increased lung infiltration of lymphocytes and neutrophils results in inflammation. This study showed that the numbers of white blood cells, lymphocytes, neutrophils, and eosinophils increased significantly after the instillation of PM<sub>2.5</sub> in the BALF of the model group ( $p < 0.01$ ). In addition, compared to the model group, the number of white blood cells in BALF of the GSE-treatment groups tended to decrease, indicating alleviation of lung inflammation and injury.

IL-1 $\beta$  is an essential pro-inflammatory factor and a sensitive indicator of the early inflammatory response that activates endothelial cells in the airways, accelerating the adhesion of eosinophils and other inflammatory cells.<sup>17</sup> It promotes the release of molecules involved in the pathogenesis of allergic inflammation of the airways.<sup>18</sup> IL-1 $\beta$  not only enters the blood but also acts on epithelial cells and mac-

rophages in the airways, inducing activation of nuclear factor- $\kappa$ B, a transcription factor essential for inflammatory responses, to promote the expression of the eotaxin gene.<sup>19</sup> Produced by monocytes, IL-10 inhibits the production of cytokines by activated macrophages.

T helper cells down-regulate the inflammatory response by effectively inhibiting the release of tumor necrosis factor- $\alpha$  (TNF- $\alpha$ ) by eosinophils, as excessive inflammation causes cellular damage.<sup>20</sup> The results of the present study showed that the content of IL-1 $\beta$  in BALF of rats in the model group was significantly higher than that in the control group ( $p < 0.01$ ), while the IL-1 $\beta$  content in the GSE-treatment groups showed a significant downward trend as compared to the model group ( $p < 0.05$ ), indicating reduced inflammatory damage. Compared to the control group, the content of IL-10 in BALF of rats in the model group was considerably reduced ( $p < 0.05$ ), while there was no significant difference between the model and GSE-treatment groups.

Histopathological analysis revealed that the lung tissue structure was relatively complete in the control group, although mild infiltration of inflammatory cells with the interstitial matter was observed in scattered cases, the distribution of alveoli was relatively uniform, and there were no significant morphological changes. The lung tissue of the model group presented infiltration and proliferation of interstitial cells, abnormal expansion of alveoli and rupturing to form a larger vesicular cavity, a significant increase in phagocytes, which were dark brown due to the aggregation of foreign particles, and a significant increase in the extent of lesions as compared to the control group. Compared to the model group, interstitial inflammation, fibrosis, and the number of phagocytes were significantly improved in the high-dose GSE group.



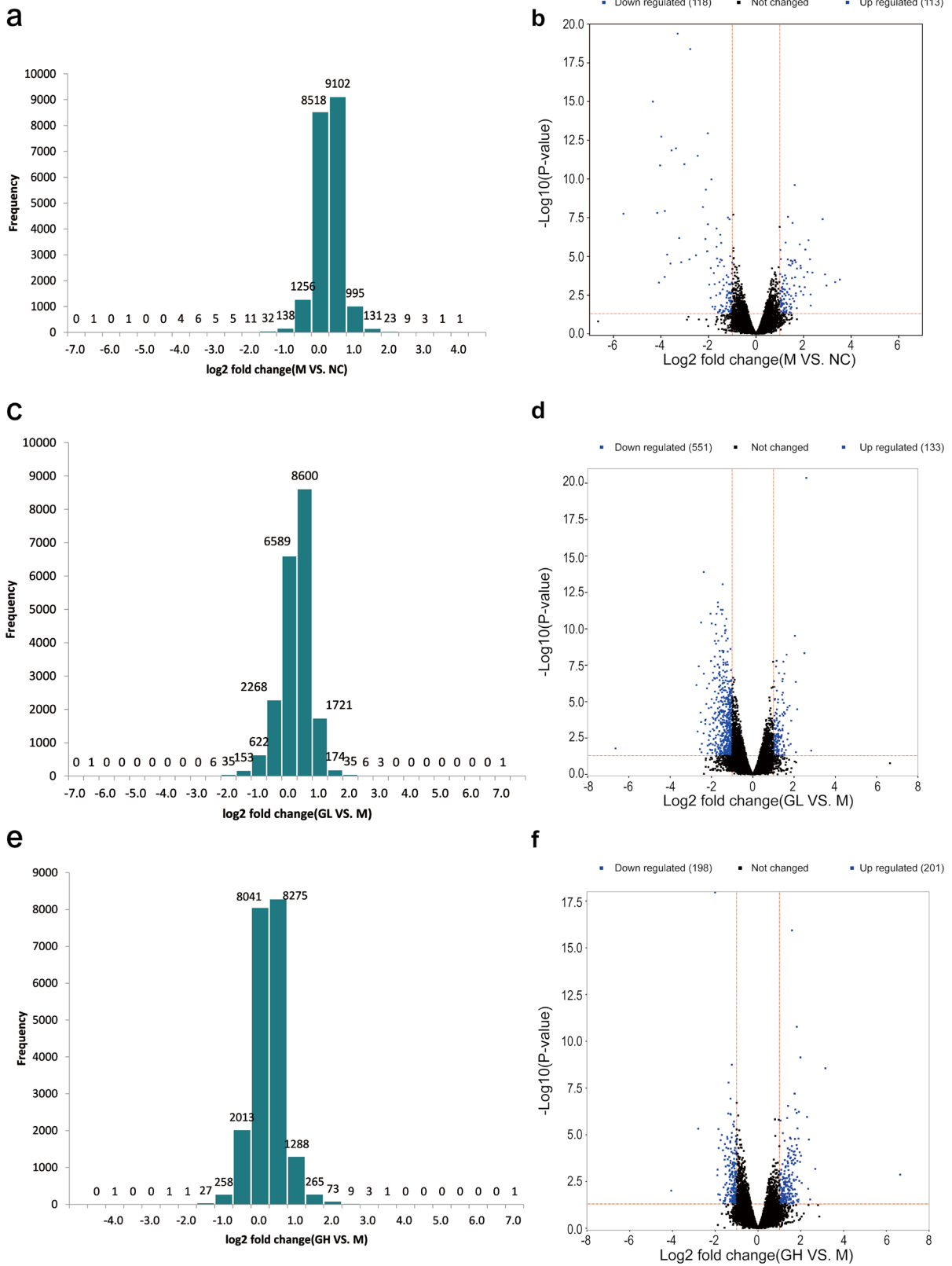


**Fig. 7. Histograms and volcano plots of DEGs.** (a) Model group vs. control group (113 upregulated, 118 downregulated). (b) Low-dose GSE group vs. model group (133 upregulated, 551 downregulated). (c) High-dose GSE group vs. model group (200 upregulated, 199 downregulated). GSE, grape skin extract.

Arginine is an intermediate metabolite of the ornithine cycle that promotes the conversion of ammonia into urea, thereby reducing blood ammonia levels.<sup>21</sup> Arginine can effectively improve immunity by promoting the secretion of natural killer cells, phagocytes, interleukin-1 (IL-1), and other endogenous substances, which is conducive to limiting the proliferation of cancer cells and preventing viral infections.<sup>22</sup> In addition, hydrolysis of arginine by arginase produces urea and ornithine, which serves as a precursor for the synthesis of L-ornithine and L-proline. Proline is a vital element of collagen; thus, supplementing arginine can promote tissue repair after severe trauma and burns, reducing inflammation and infection risk. Furthermore, L-arginine is the only substrate for the synthesis of nitric oxide, which is an important biological messenger that promotes the activation of natural killer cells and monocytes in the peripheral blood. It regulates the secretion of cytokines by T lymphocytes and macrophages, thus playing an essential role in the immune response.<sup>9</sup> GSE administration tended to increase the content of L-arginine and improved the immune response by promoting the activation of natural killer cells and phagocytes.

Phosphatidylcholine (1,2-diacyl-sn-glycero-3-phosphocholine) is an amphoteric molecule consisting of a hydrophilic head and a hydrophobic tail. Studies have shown that exposure to atmospheric PM2.5 can damage alveolar epithelial type II cells and limit mechanical stretching, indicating dysfunction in synthesizing the surfactant substance phosphatidylcholine. Deficiency of the pulmonary surfactant phosphatidylcholine leads to increased alveolar surface tension and dysregulation of the gas-fluid interface, thereby reducing the fluidity of cell membranes and altering cell signal conduction, leading to single-molecule layer damage, septal rupture, and alveolar cavity fusion.<sup>23–25</sup> In addition, the hemolytic phosphatidylcholine is involved in eosinophil infiltration, which promotes inflammation, increases respiratory resistance, and reduces the release of pro-inflammatory cytokines associated with TNF- $\alpha$ .<sup>26</sup> The results of this study showed that the reduction of phosphatidylcholine in the lung tissue of the rats in the model group might lead to abnormal function of surfactants, the increased surface tension of alveoli, dysfunction of the gas-liquid interface, reduced fluidity of cell membranes, and interrupted conduction of cell signals, resulting in monolayer damage, diaphragm rupture, and alveolar cavity fusion. The correlation between these findings and the histology data suggests that lung damage caused by PM2.5 is directly related to alterations in the phospholipid content of the cells that line the lung surface. Administration of GSE tended to increase the phosphatidylcholine content, which may have improved PM2.5-induced lung damage. Thus, future studies are warranted to explore the underlying mechanisms further.

A gene chip to assess mRNA expression profiles showed that PM2.5-induced damage to the rat lung is likely due to chemokine signaling pathways, the peroxisome proliferation activation receptor signaling pathway, tumor necrosis factor signaling pathway, lipolysis regulatory signaling pathway of fat cells, and AMP-dependent protein kinase signaling pathway, while GSE improved lung function via the complement system and oxidative phosphorylation pathway. However, future studies are needed to elucidate the specific mechanisms.

### Future directions

A grape skin seed extract has been shown to help with anti-aging and gut microbiota regulation. In addition, our research group found that it had an excellent preventive effect on lung injury induced by artificial fine particulate matter and explored its possible

mechanism through multi-omics. However, our team has not yet conducted a more in-depth exploration of the enriched drug action pathways in the whole research process. In future research, we will focus on exploring the related pathways of drug action to use drugs more rationally.

### Conclusions

In summary, the mechanism of action of rat lung injury caused by PM2.5 may be a comprehensive effect produced by the joint actions of multiple pathways. GSE significantly improved lung function and inflammation caused by PM2.5. The amino acids and lipid substances detected in this study provide vital information for subsequent in-depth studies to elucidate potential targets and the intervention mechanism of GSE.

### Acknowledgments

Special thanks to Professor Zhongze Fang for his great support and help in metabonomics detection and Professor Hong Yang for her great support and help in transcriptomics detection.

### Funding

This study was financially supported by the National Natural Science Foundation of China (grant no. 82074104), the Chinese Academy of Medical Sciences-CAMS Innovation (grant no. CAMS-I2M), and the Chinese Society of Toxicology (grant no. CST2021CT101), Discipline Construction Project of Peking Union Medical College (grant number: 201920200801).

### Conflict of interest

HTJ has been an editorial board member of *Future Integrative Medicine* since November 2021. The other authors declare that they have no conflict of interest related to this publication.

### Author contributions

Conception and design (HTJ and PCZ); Administrative support (HTJ and PCZ); Provision of study materials or patients (HTJ, PCZ, JB, and JL); Collection and assembly of data (YHL, ZGL, SZL, HYJ, and LK); Data analysis and interpretation (ZGL, YHL, SZL, HYJ, and LK); Manuscript composition: All authors; Final approval of manuscript: All authors.

### Ethical Statement

The animal test has been approved by the Center for Beijing Union-Genius Pharmaceutical Technology Development Co. Ltd. Ethical Approval No.: 2017-0000242. The protocol was approved by the Center for Beijing Union-Genius Pharmaceutical Technology Development Co. Ltd., and the procedures followed the approved guidelines. All animals were euthanized using CO<sub>2</sub> gas in a special chamber, and all efforts were made to minimize suffering.

### Data sharing statement

The data used in supporting the findings of this study are included within the article.

## References

- [1] Yang L, Li C, Tang X. The Impact of PM2.5 on the Host Defense of Respiratory System. *Front Cell Dev Biol* 2020;8:91. doi:10.3389/fcell.2020.00091, PMID:32195248.
- [2] Timmis A, Vardas P, Townsend N, Torbica A, Katus H, De Smedt D, *et al*. European Society of Cardiology: cardiovascular disease statistics 2021. *Eur Heart J* 2022;43(8):716–799. doi:10.1093/eurheartj/ehab892, PMID:35016208.
- [3] Chen W, Chen S, Zhao L, Zhang M, Geng H, Dong C, *et al*. Effects of real-ambient PM2.5 exposure plus lipopolysaccharide on multiple organ damage in mice. *Hum Exp Toxicol* 2022;41:9603271211061505. doi:10.1177/09603271211061505, PMID:35098763.
- [4] Guo H, Li W, Wu J. Ambient PM2.5 and Annual Lung Cancer Incidence: A Nationwide Study in 295 Chinese Counties. *Int J Environ Res Public Health* 2020;17(5):1481. doi:10.3390/ijerph17051481, PMID:32106556.
- [5] Waidyatillake NT, Campbell PT, Vicendese D, Dharmage SC, Curto A, Stevenson M. Particulate Matter and Premature Mortality: A Bayesian Meta-Analysis. *Int J Environ Res Public Health* 2021;18(14):7655. doi:10.3390/ijerph18147655, PMID:34300107.
- [6] Bu X, Xie Z, Liu J, Wei L, Wang X, Chen M, *et al*. Global PM2.5-attributable health burden from 1990 to 2017: Estimates from the Global Burden of disease study 2017. *Environ Res* 2021;197:111123. doi:10.1016/j.envres.2021.111123, PMID:33823194.
- [7] Kopf M, Schneider C, Nobs SP. The development and function of lung-resident macrophages and dendritic cells. *Nat Immunol* 2015;16(1):36–44. doi:10.1038/ni.3052, PMID:25521683.
- [8] Yan XD, Wang QM, Tie C, Jin HT, Han YX, Zhang JL, *et al*. Polydatin protects the respiratory system from PM2.5 exposure. *Sci Rep* 2017;7:40030. doi:10.1038/srep40030, PMID:28067267.
- [9] Liu T, Zhang P, Ling Y, Hu G, Gu J, Yang H, *et al*. Protective Effect of Colla corii asini against Lung Injuries Induced by Intratracheal Instillation of Artificial Fine Particles in Rats. *Int J Mol Sci* 2018;20(1):55. doi:10.3390/ijms20010055, PMID:30583600.
- [10] de F C Lichtenfels AJ, van der Plaats DA, de Jong K, van Diemen CC, Postma DS, Nedeljkovic I, *et al*. Long-term Air Pollution Exposure, Genome-wide DNA Methylation and Lung Function in the LifeLines Cohort Study. *Environ Health Perspect* 2018;126(2):027004. doi:10.1289/EHP2045, PMID:29410382.
- [11] Bergstra AD, Brunekreef B, Burdorf A. The effect of industry-related air pollution on lung function and respiratory symptoms in school children. *Environ Health* 2018;17(1):30. doi:10.1186/s12940-018-0373-2, PMID:29587756.
- [12] Guo C, Zhang Z, Lau AKH, Lin CQ, Chuang YC, Chan J, *et al*. Effect of long-term exposure to fine particulate matter on lung function decline and risk of chronic obstructive pulmonary disease in Taiwan: a longitudinal, cohort study. *Lancet Planet Health* 2018;2(3):e114–e125. doi:10.1016/S2542-5196(18)30028-7, PMID:29615226.
- [13] Gripenbäck S, Lundgren L, Eklund A, Lidén C, Skare L, Tornling G, *et al*. Accumulation of eosinophils and T-lymphocytes in the lungs after exposure to pinewood dust. *Eur Respir J* 2005;25(1):118–124. doi:10.1183/09031936.04.00059804, PMID:15640332.
- [14] Sigaud S, Goldsmith CA, Zhou H, Yang Z, Fedulov A, Imrich A, *et al*. Air pollution particles diminish bacterial clearance in the primed lungs of mice. *Toxicol Appl Pharmacol* 2007;223(1):1–9. doi:10.1016/j.taap.2007.04.014, PMID:17561223.
- [15] Foster MW, Morrison LD, Todd JL, Snyder LD, Thompson JW, Soderblom EJ, *et al*. Quantitative proteomics of bronchoalveolar lavage fluid in idiopathic pulmonary fibrosis. *J Proteome Res* 2015;14(2):1238–1249. doi:10.1021/pr501149m, PMID:25541672.
- [16] Kendall M, Guntern J, Lockyer NP, Jones FH, Hutton BM, Lippmann M, *et al*. Urban PM2.5 surface chemistry and interactions with bronchoalveolar lavage fluid. *Inhal Toxicol* 2004;16:115–129. doi:10.1080/08958370490443204, PMID:15204800.
- [17] Castañeda AR, Pinkerton KE, Bein KJ, Magaña-Méndez A, Yang HT, Ashwood P, *et al*. Ambient particulate matter activates the aryl hydrocarbon receptor in dendritic cells and enhances Th17 polarization. *Toxicol Lett* 2018;292:85–96. doi:10.1016/j.toxlet.2018.04.020, PMID:29689377.
- [18] Xu F, Qiu X, Hu X, Shang Y, Pardo M, Fang Y, *et al*. Effects on IL-1 $\beta$  signaling activation induced by water and organic extracts of fine particulate matter (PM<sub>2.5</sub>) *in vitro*. *Environ Pollut* 2018;237:592–600. doi:10.1016/j.envpol.2018.02.086, PMID:29525626.
- [19] Li X, Geng J, Chen Y, Chen F, Liu C, Xu Q, *et al*. Exposure to particulate matter induces cardiomyocytes apoptosis after myocardial infarction through NF $\kappa$ B activation. *Biochem Biophys Res Commun* 2017;488(1):224–231. doi:10.1016/j.bbrc.2017.05.047, PMID:28499868.
- [20] Wong TH, Lee CL, Su HH, Lee CL, Wu CC, Wang CC, *et al*. A prominent air pollutant, Indeno[1,2,3-cd]pyrene, enhances allergic lung inflammation via aryl hydrocarbon receptor. *Sci Rep* 2018;8(1):5198. doi:10.1038/s41598-018-23542-9, PMID:29581487.
- [21] Guan L, Geng X, Shen J, Yip J, Li F, Du H, *et al*. PM2.5 inhalation induces intracranial atherosclerosis which may be ameliorated by omega 3 fatty acids. *Oncotarget* 2018;9(3):3765–3778. doi:10.18632/oncotarget.23347, PMID:29423081.
- [22] Kim HB, Eckel SP, Kim JH, Gilliland FD. Exhaled NO: Determinants and Clinical Application in Children With Allergic Airway Disease. *Allergy Asthma Immunol Res* 2016;8(1):12–21. doi:10.4168/aair.2016.8.1.12, PMID:26540497.
- [23] Takayama N, Iwamoto N, Sumi D, Shinkai Y, Tanaka-Kagawa T, Jinno H, *et al*. Peroxiredoxin 6 is a molecular target for 1,2-naphthoquinone, an atmospheric electrophile, in human pulmonary epithelial A549 cells. *J Toxicol Sci* 2011;36(6):817–821. doi:10.2131/jts.36.817, PMID:22129745.
- [24] Coccini T, Manzo L, De Simone U, Acerbi D, Roda E. Novel tools for blood inflammatory markers detection in monitoring air pollution-induced cardio-respiratory symptoms. *G Ital Med Lav Ergon* 2012;34(2):175–86. PMID:22888728.
- [25] Chen WL, Lin CY, Yan YH, Cheng KT, Cheng TJ. Alterations in rat pulmonary phosphatidylcholines after chronic exposure to ambient fine particulate matter. *Mol Biosyst* 2014;10(12):3163–3169. doi:10.1039/c4mb00435c, PMID:25236678.
- [26] Ballou LR, Lauderkind SJ, Rosloniec EF, Raghov R. Ceramide signalling and the immune response. *Biochim Biophys Acta* 1996;1301(3):273–287. doi:10.1016/0005-2760(96)00004-5, PMID:8664339.